Journal of Materials Science: Materials in Electronics
https://doi.org/10.1007/s10854-017-8508-8

Influence of the sintering process on ferroelectric properties of $Bi_{0.5}(Na_{0.8}K_{0.2})_{0.5}TiO_3$ lead-free piezoelectric ceramics

J. Camargo[1] · A. Prado Espinosa[1] · L. Ramajo[1] · M. Castro[1]

Received: 12 July 2017 / Accepted: 29 December 2017

Abstract
The effect of sintering process, particularly the sintering time, on ferroelectric properties of $Bi_{0.5}(Na_{0.8}K_{0.2})_{0.5}TiO_3$ (BNKT) has been studied and compared with $Bi_{0.5}Na_{0.5}TiO_3$ (BNT) and $Bi_{0.5}K_{0.5}TiO_3$ (BKT) ceramics. Ceramic powders were prepared by the solid-state reaction method, employing a mechanochemical activation step, and sintered at different times. Samples were characterized by X-ray diffraction (XRD), Raman microspectroscopy, Scanning Electron Microscopy (SEM), impedance spectroscopy and ferroelectric hysteresis loops. Through XRD and Raman results, the perovskite structure was detected. In addition, a secondary phase was observed by SEM images. As the sintering time was increased, the medium grain size grew, and the amount of the secondary phase raised. Moreover, dielectric properties were modified by the resulting grain size and the amount of the secondary phase.

1 Introduction

Piezoelectric ceramics are widely used for many applications such as sensors, actuators, and transducers due to their electromechanical properties. In this way, lead titanate–zirconate piezoceramics are the most extensively used materials for these devices, although lead toxicity is a serious threat to human health and environment [1]. Therefore, considerable efforts, regulations and restrictions on using hazardous substances in electronic devices have been devoted towards the development of lead-free piezoelectric ceramics.

Recent reports on lead-free piezo-ceramics can be categorized into two main perovskite families: $(K,Na)NbO_3$ (KNN) and $(Bi, Na)TiO_3$ (NBT) or $(Bi,K)TiO_3$ (BKT) [2–4]. $K_{0.5}Na_{0.5}NbO_3$ (KNN) system has attracted much attention, due to its elevated Curie temperature (about 420 °C) and high piezoelectric properties close to the morphotropic phase boundary (MPB) [5]. Nevertheless, it is difficult to obtain pure KNN-based ceramics with high density and great piezoelectric performance.

Sodium bismuth titanate $Na_{0.5}Bi_{0.5}TiO_3$ (BNT) with relatively large remnant polarization at room temperature and high Curie temperature could be considered as a promising candidate to lead-free piezoelectric ceramics [6]. The high strain observed in the BNT system under a strong electric field is due to the 90° domain reorientation [7] which increases the coercive field and hinders the development of desired piezoelectric properties. Consequently, numerous studies have been carried out to improve electrical properties of BNT by the formation of solid solutions with other ABO_3 perovskites [8–10]. In fact, the partial substitution of sodium by potassium in $Bi_{0.5}Na_{0.5}TiO_3$–$Bi_{0.5}K_{0.5}TiO_3$ (BNKT) systems results in ceramics with ferroelectric properties [11] due to the formation of a rhombohedral–tetragonal morphotropic phase boundary (MPB) at the optimal composition of $Bi_{0.5}(Na_{0.8}K_{0.2})_{0.5}TiO_3$ [9]. In a previous work, the formation of a secondary phase of composition close to $K_{2-x}Na_xTi_6O_{13}$ was observed [12]. This phase was detected when samples were sintered at temperatures higher than 1100 °C and its formation was associated with the mechanochemical activation of powders in the solid-state reaction method.

In this work, we present a facile method to prepare $Bi_{0.5}(Na_{1-x}K_x)_{0.5}TiO_3$-based lead-free piezoelectric ceramics by the solid-state reaction method using a previous mechanochemical activation step of reagents. The main achievement is the clarification of the effect of the sintering time on the structure, microstructure, dielectric and piezoelectric properties of $Bi_{0.5}(Na_{0.8}K_{0.2})_{0.5}TiO_3$-based system and compared with BNT and BKT ceramics. It should be emphasized that when the sintering time is increased, the grain size and

✉ J. Camargo
jcamargo@fi.mdp.edu.ar

[1] Institute of Research in Materials Science and Technology (INTEMA), Juan B. Justo 4302, B7608FDQ Mar del Plata, Argentina

Published online: 03 January 2018

the content of secondary phases increases. Consequently, piezoelectric and dielectric properties of these ceramics were influenced by the sintering time.

2 Experimental procedure

$Bi_{0.5}(Na_{0.8}K_{0.2})_{0.5}TiO_3$ (BNKT), $Bi_{0.5}Na_{0.5}TiO_3$ (BNT) and $Bi_{0.5}K_{0.5}TiO_3$ (BKT) were synthesized through solid state reaction, using K_2CO_3 and Na_2CO_3 (Aldrich 99.5%; USA), Bi_2O_3 (Aldrich 99.8%; USA) and TiO_2 (Aldrich 99.9%; USA). Powders were mixed and milled using zirconia balls in an alcoholic medium for 3 h in a planetary mill (Fritsch, Pulverisette 7, 1010 rpm). Powders were dried and calcined at700 °C for 2 h. The resulting powders were milled again and pressed into disks. In order to improve samples densification and to avoid alkaline volatilization, particularly potassium, sintering temperatures were selected taken into account previous studies reported in literature [12]. Disks of BNKT were sintered at 1100 °C for 2, 5 or 8 h (hereafter, denoted as BNKT-2, BNKT-5 and BNKT-8), disks of BNT were sintered at 1150 °C for 2 h, and disks of BKT were sintered at 1025 for 2 h.

Crystalline phases were characterized by X-ray diffraction (XRD) (XRD, PANalytical, X'pert Pro, CuK_α). Density values were determined using the Archimedes' method. Ceramic samples were polished and grain boundaries were highlighted through a chemically etching step employing a solution of HCl and HF. Etched samples were analyzed by Scanning Electron Microscope, SEM (Jeol JSM-6460LV).

Raman microspectrometric analyses of samples were performed on a multichannel Renishaw In Via Reflex microspectrometer. Excitation was provided by the 514 nm line of a Ar laser. To achieve enhanced signal-to-noise ratio, 30–50 scans were accumulated, each of 15 s exposure time with laser power ranging between 30 and 300 mW.

Before the electrical measurements, a fired silver paste was used for the electric contacts. The temperature dependence of the dielectric properties was determined using an impedance analyzer (Hewlett–Packard, HP4284A) over a frequency range of 20 Hz–1 MHz. Samples were polled in a silicone oil bath at 100 °C by applying a DC field of 30.0 kV/cm for 10 min. The piezoelectric constant d_{33} was measured using a piezo d_{33} meter (YE2730A d_{33} METER, APC International, Ltd., USA). The polarization–electric field (P–E) hysteresis loops were measured in a silicon oil bath using a modified Sawyer–Tower circuit. The electromechanical planar coupling factor (Kp) was calculated from the impedance curves of the polarized ceramics, according to Eq. 1 [13].

$$K_p = \sqrt{2.51 \times \left\{ \frac{(f_a - f_r}{f_a} \right\}} \quad (1)$$

where, f_a is the anti-resonance frequency and f_r is the resonance frequency.

3 Results and discussion

As mentioned before ceramics were sintered for different times (2, 5, 8 h) in order to establish the sintering time influence on final properties of the BNKT system and compared with sintered BNT and BKT samples. XRD patterns of sintered samples are shown in Fig. 1. All patterns can be assigned to a perovskite structure associated with BNT (JCDS No 36-0340), BKT (JCDS No 36-0340) and a BNKT calculated pattern [14], respectively. Moreover, BNKT peaks are displaced between BNT and BKT peaks. After analyzing the peaks of sintered samples located between $39.5° < 2\theta < 40.5°$ and $46° < 2\theta < 47°$, the diminution of the 39.83° and 46.43° peaks can be attributed to the pseudocubic structure, while the increase of 40.00° to 40.09°, and 46.52° to 46.64° peaks are related to the rhombohedral structure. Consequently, XRD patterns suggest the rhombohedral structure stabilization as the sintering time is increased. Additionally, the full-width at half-maximum peak (FWHW) decreases with increasing sintering time, which is attributed to the increasing grain size.

Figure 2 shows Raman spectra of BNT, BNKT (2, 5 and 8 h) and BKT samples. Raman results agree with previously reported data. Peaks around 240 and 400 cm^{-1} could be attributed to the K–O–Ti stretching containing short Ti–O bonds, whereas bands at 615 cm^{-1}, approximately, can be assigned to the Ti–O–Ti stretch in edge-shared TiO_6. Bands close to 870 cm^{-1} are related to a short Ti–O stretching vibration in distorted TiO_6. Broad bands due to the A-site disorder structure and to different Raman-modes overlapped are observed [15].

In addition, differences between BKT, BNT and BNKT are observed. From 200 to 400 cm^{-1}, the overlapping into three bands in BKT is detected (210, 275, 345 cm^{-1}). Moreover, two BKT Raman bands (525 and 635 cm^{-1}) are separated between 400 and 700 cm^{-1}. However, in BNT samples only two overlapped bands are observed between 200 and 400 cm^{-1} (273 and 295 cm^{-1}) and the overlapping of bands located at 535 and 577 cm^{-1} is observed. These modifications can be assigned to differences in the K–O–Ti and Na–O–Ti stretching vibration. The K^+ cations compete with Na^+ in the occupancy of A sites of the ABO_3 perovskite to form a solid solution. The large distortion caused by the incorporation of K^+ cations modified the structure of the solid solution. Clearly, the position of bands associated with Na–O–Ti to higher wavenumber when potassium is incorporated can be assigned to an increase in the bond strength caused by the shortening of the distance between B^{5+}-type ions and oxygen. Contrary, bands located between 700 and

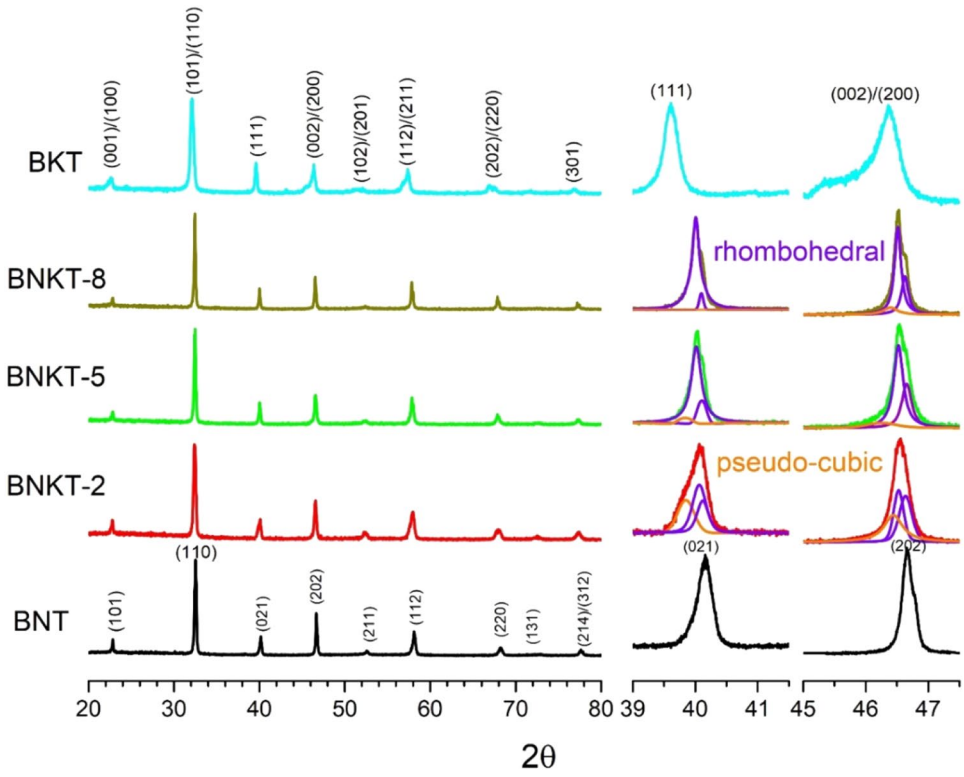

Fig. 1 XRD patterns of sintered samples. All peaks are associated with the perovskite phase. The inserts of the Figure show the magnified XRD diffraction patterns in the 2Θ range 39° to 41° and 46 to 47°

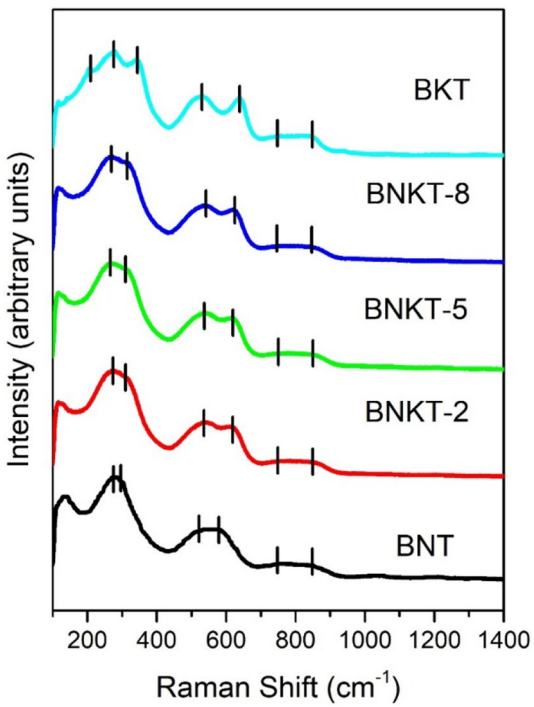

Fig. 2 Raman spectra of BNT, BNKT-2, -5, -8 and BKT samples

900 cm^{-1}, which are associated with a short Ti–O stretching vibration in distorted TiO_6, do not show differences in all samples.

Although Raman spectra of BNKT-based ceramics match between the ones of BNT and BKT-based samples, the structure evolution during sintering time cannot be established from these spectra.

The SEM images, Fig. 3a–e, illustrates the microstructure of the BNT (a), BNKT sintered during 2 to 8 h (b–d) and BKT (e) ceramics. The average grain size increases from BKT, BNKT to BNT. Furthermore, in BNKT samples, a secondary phase with bar-like morphology is detected. As the sintering time is increased, the secondary phase growths without the formation of new nucleus (see Fig. 3c, d). Contrary, in the sample sintered for 8 h (Fig. 3e), new nucleus of this secondary phase are dispersed throughout the sample. This secondary phase, was previously observed by authors and it was established that the amount of this phase, attributed to $K_{2-x}Na_xTi_6O_{13}$, increased with the sintering temperature [12].

Figure 4 shows magnifications of SEM images of BNKT-2, -5 and -8 samples. It can be observed, that the average grain size increases from 0.55 μm in samples sintered for 2 h, to 0.85 in samples sintered for 5 h, and to 1.1 μm for samples sintered for 8 h. Taking into account the microstructural analyses and XRD results, it can be inferred that the reduced grain size of sintered samples for 2 h favors the stabilization of the pseudo-cubic structure in the main phase. On the other hand, considering that the secondary phase retains potassium ions, as the sintering time increases the main phase become potassium-less and the stoichiometry

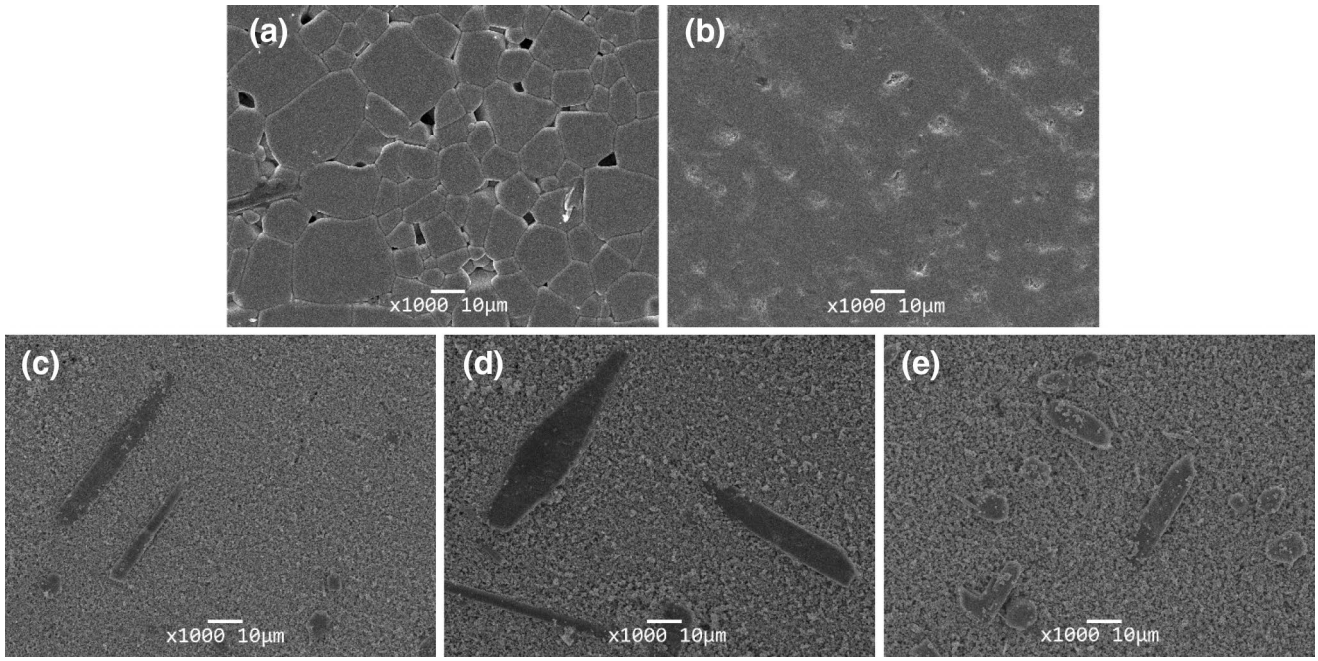

Fig. 3 SEM images of BNT (**a**), BKT (**b**), BNKT-2 (**c**), BNKT-5 (**d**) and BNKT-8 (**e**). (bar = 10 µm)

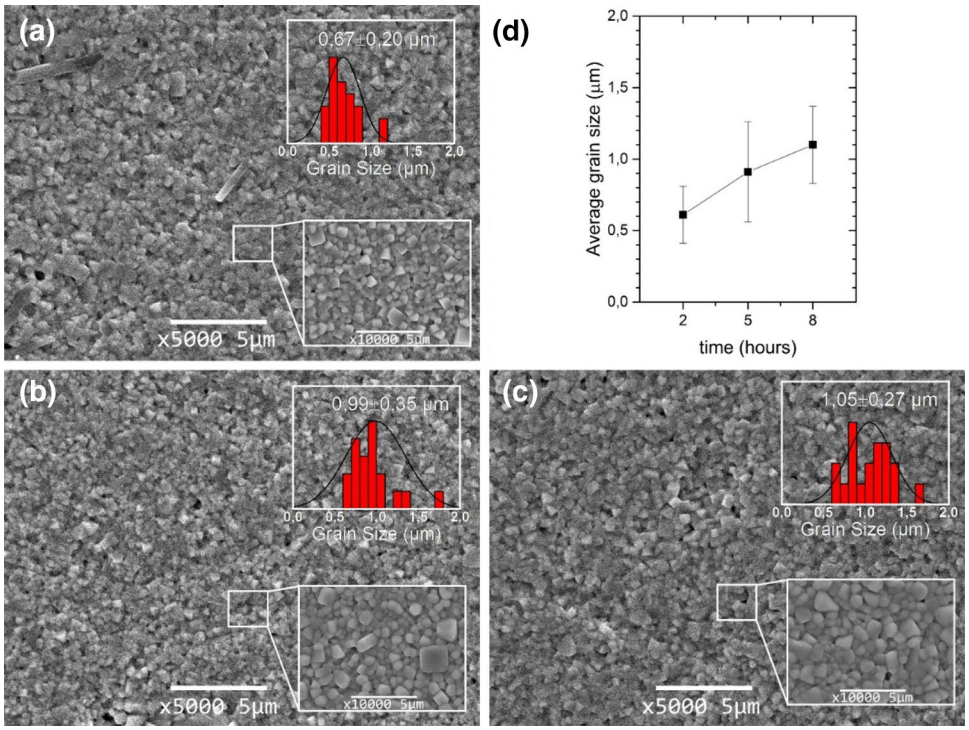

Fig. 4 SEM images of BNKT-2 (**a**), BNKT-5 (**b**) and BNKT-8 (**c**). Evolution of the average grain size is with the sintering time (**d**). (Bar = 5 µm)

and stabilized structure become similar to the ones of the BNT sample. Potassium capture by the secondary phase is responsible of the stabilized rhombohedral structure at the highest sintering time and avoids the tetragonal–rhombohedral morphotropic boundary.

Dielectric curves as function of temperature (a, b) and as function of frequency (c, d) are displayed in Fig. 5. It can be observed that depolarization temperature (T_d) is displaced to lower temperatures as the sintering temperature increases. Contrary, the maximum temperature moves to higher values

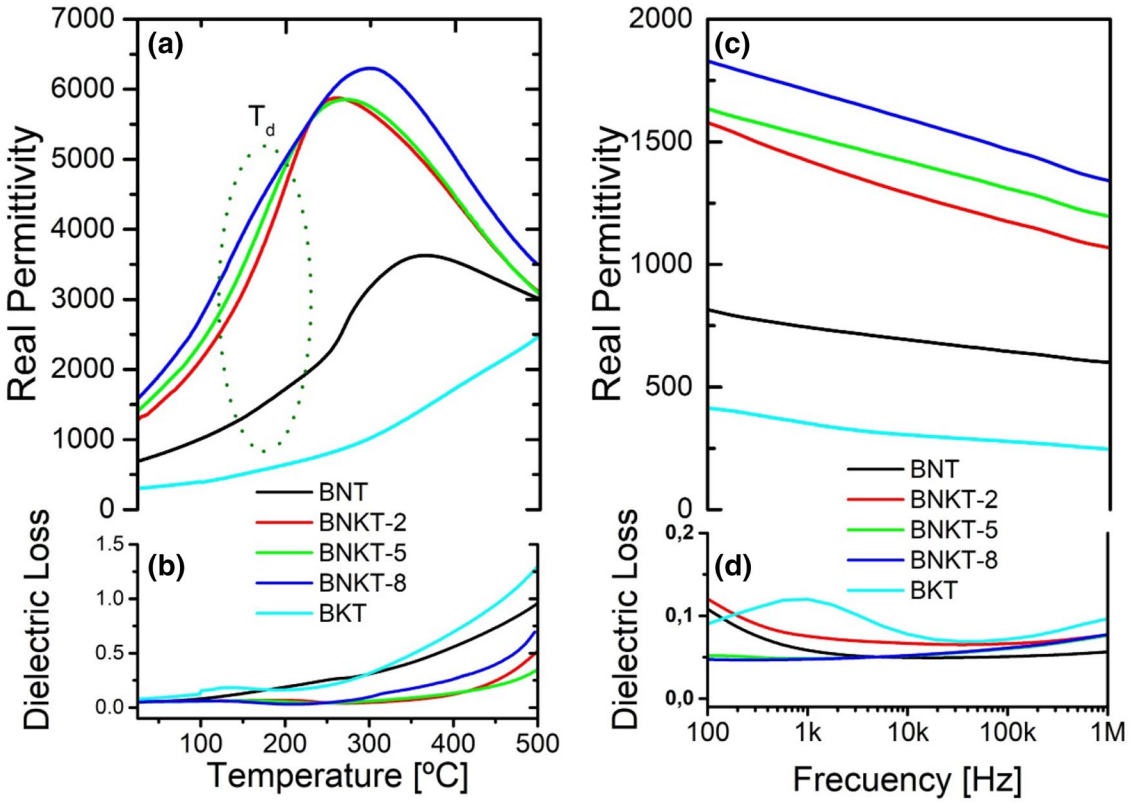

Fig. 5 **a, b** Temperature-dependence at 100 kHz, and **c, d** frequency-dependence at room temperature of dielectric permittivity (**a, c**) and dielectric loss (**b, d**) of BNT, BNKT-2 to -8 and BKT

as the sintering temperature increases. These results suggest that the increasing sintering time enhances the relaxor behavior due to the reduction of the long-range arrangement. Figure 5b shows dielectric loss curves as function of temperature. The dielectric losses rise with the sintering time, can be related to the size and content of the secondary phase.

BNKT samples exhibit higher real permittivity values than BNT samples (see Fig. 5c). BKT samples show high real permittivity values at low frequency whereas a diminution at high frequencies is observed. Furthermore, from Fig. 5d. dielectric loss of BKT samples prevents the possible use of these materials as piezoelectric devices.

Hysteresis loops of BNT and BNKT series are shown in Fig. 6. For BKT-based ceramics hysteresis loops were not obtained due to the high dielectric loss values registered. The maximum fields used in this work were limited by the equipment available in our laboratory. In order to compare the complete set of samples, the same maximum field was used for all the specimens. At room temperature BNKT samples exhibit higher remnant polarization values (Pr) 4.01, 4.78 and 3.97 μC/cm^2 (for BNKT-2, BNKT-5 and BNKT-8, respectively) than BNT samples (Pr: 0.71 μC/cm^2). Moreover, remnant polarization rises, and coercive field decreases from 14.45, 12.97 to 10.07 kV/cm when the sintering time

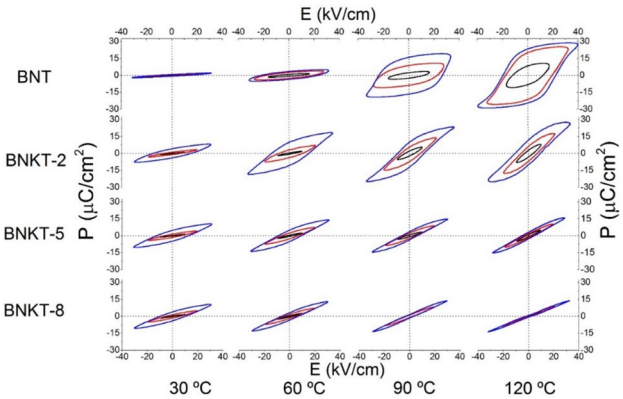

Fig. 6 Ferroelectric hysteresis loops of BNT, BNKT-2, -5, and -8 ceramics as function of temperature, measured at 50 Hz

increases. This behavior is related to the average grain growth increasing which is strongly influenced by the sintering time. Furthermore, the softening of hysteresis loops at lower temperatures can be attributed to the depolarization temperature diminution as the sintering temperature rises.

Finally, Table 1 illustrates the density, dielectrics properties, and piezoelectric constants (d_{33} and K_p) of sintered

Table 1 Density values, densification level of sintered samples, real permittivity (ε′), dielectric loss (tan δ), Piezoelectric constant (d_{33}) and electromechanical planar coupling factor (K_p) of the samples measured at 30 °C and 10 kHz

	Density (g/cm^3)	Densification level (%)	ε′	tan δ	d_{33}	K_p
BNT	5.620	94.60	590	0.045	87	0.21
BNKT-2 h	5.755	96.40	941	0.082	108	0.20
BNKT-5 h	5.768	96.61	1059	0.059	111	0.19
BNKT-8 h	5.785	96.89	1075	0.064	58	0.17
BKT	5.681	96.50	1260	3.57	–	–

samples. Samples sintered for 8 h presents the highest density value, whereas the highest piezoelectric constant is registered in samples sintered for 5 h. Moreover, piezoelectric constant is reduced in samples sintered for 8 h due to the influence of the secondary phases which modifies the composition of the main phase. Electromechanical planar coupling factor decreases as the sintering time is increased due to the influence of the secondary phase. Taking into account piezoelectric constant, electromechanical coupling factor and densification level, optimum properties are achieved in BNKT samples sintered for 5 h. Furthermore, although sintering temperature of BKT is 75 °C lower than the sintering temperature of BNKT, the final densification level of both samples is similar. This result is indicative of the right temperature selection for this comparative study.

4 Conclusions

The influence of the sintering process on ferroelectric properties of $Bi_{0.5}(Na_{0.8}K_{0.2})_{0.5}TiO_3$ lead-free piezoelectric ceramics has been reported. Ceramic powders were prepared by the solid-state reaction method employing a mechanochemical activation step and sintered for different times. The increasing in the sintering time favored the grain growth of the main phase and the development of the secondary phase. From electron microscopy analyses and XRD patterns the formation of a secondary phase and the evolution of the main phase from pseudocubic to rhombohedral structure avoiding the stabilization of the morphotropic phase boundary was confirmed. Furthermore, the secondary phase captured potassium ions and the main phase composition and structure become close to the ones of the BNT-sample.

Dielectric and piezoelectric properties were influenced by modifications in the structure and microstructure evolution with sintering time. Certainly, samples sintered for 5 h registered an improvement in the piezoelectric constant whereas a diminution was observed in samples sintered for 8 h. Additionally, as the sintering time was raised, the long-range arrangement and the depolarization temperature were reduced and ferroelectric properties were softened.

To sum up, dielectric and piezoelectric properties in BNKT-based ceramics were increased when the sintering time favored the grain size growth, the main phase composition was not substantially modified by the formation of the secondary phase, and the rhombohedral structure was not completely stabilized.

Acknowledgements The authors thank the following institutions for providing financial support: National Research Council (CONICET, Argentina) PIP 2012-0432, National Agency of Scientific and Technological Promotion (ANPCYT, Argentina) PICT 2014-1314, and National University of Mar del Plata (Argentina) Project (15G/388).

References

1. J. Rödel, W. Jo, K.T.P. Seifert, E.M. Anton, T. Granzow, D. Damjanovic, J. Am. Ceram. Soc. **92**, 1153 (2009)
2. X.P. Jiang, L.Z. Li, M. Zeng, H.L.W. Chan, Mater. Lett. **60**, 1786 (2006)
3. J.B. Lim, S. Zhang, J.-H. Jeon, T.R. Shrout, J. Am. Ceram. Soc. **93**, 1218 (2010)
4. K.S.T. Takenaka, K. Maruyama, Jpn. J. Appl. Phys. **30**(Part 1), 2236 (1991)
5. R. Wang, R. Xie, T. Sekiya, Y. Shimojo, Mater. Res. Bull. **39**, 1709 (2004)
6. P. Fu, Z. Xu, R. Chu, W. Li, X. Wu, M. Zhao, Mater. Chem. Phys. **138**, 140 (2013)
7. K.N. Pham, A. Hussain, C.W. Ahn, W. Kim, S.J. Jeong, J.S. Lee, Mater. Lett. **64**, 2219 (2010)
8. M. Jiang, X. Liu, C. Liu, Mater. Res. Bull. **45**, 220 (2010)
9. B. Wang, L. Luo, F. Ni, P. Du, W. Li, H. Chen, J. Alloys Compd. **526**, 79 (2012)
10. Z. Chong-rong, C. Li-yuan, Bull. Mater. Sci. **34**, 933 (2011)
11. A. Ullah, R.A. Malik, A. Ullah, D.S. Lee, S.J. Jeong, J.S. Lee, I.W. Kim, C.W. Ahn, J. Eur. Ceram. Soc. **34**, 29 (2014)
12. L. Ramajo, J. Camargo, F. Rubio-Marcos, M. Castro, Ceram. Int. **41**, 5380 (2015)
13. J.-F. Trelcat, C. Courtois, M. Rguiti, A. Leriche, P.-H. Duvigneaud, T. Segato, Ceram. Int. **38**, 2823 (2012)
14. G.O. Jones, J. Kreisel, P.A. Thomas, Powder Diffr. **17**, 301 (2002)
15. J. Kreisel, aM. Glazer, G. Jones, P. Thomas, L. Abello, G. Lucazeau, J. Phys. Condens. Matter. **12**, 3267 (2000)